JCE

JOURNAL OF
CIVIL ENGINEERING
ISSN 2086 - 1206 E-ISSN 2579 - 9029

Vibration Characteristics of Long-span Reinforced Concrete Hollow Flat Slabs: A Case Study

Li Zhou[a*], Yong Huang[b], Bo Chen[a]

Correspondence

[a]College of Architecture and Urban Planning, Guizhou University, Guiyang 550003, China.
[b]Architectural survey and design institute, Guizhou University, Guiyang 550003, China.

Corresponding author email adress:
lzhou5@gzu.edu.cn

Submitted : 4 May 2026
Revised : 13 June 2026
Accepted : 20 June 2026

Abstract

To investigate the vibration characteristics of the long-span reinforced concrete hollow flat slab, an actual engineering case was studied to examine the influence of parameters such as slab thickness and supporting beam cross-sectional dimensions on the dynamic properties of the floor. The dynamic response under human-induced loading was also analyzed. The study found that the thickness of floor slabs in the long-span zone significantly affects their fundamental frequency. As the total slab thickness varies from 450 mm to 850 mm, the fundamental frequency ranges from 5.043 Hz to 7.847 Hz, representing a 55.6% increase from the minimum value to the maximum. In contrast, the slab thickness in non-long-span zones and the cross-sectional dimensions of the supporting beams have a relatively small influence on the fundamental frequency. Both the magnitude and duration of the single-step gravity load influence the peak acceleration and vertical displacement of the floor. When the applied gravity load increases from 0.4 kN to 0.8 kN, the peak acceleration and maximum vertical displacement increase by 100.8% and 100.2%, respectively. When the load duration increases from 0.4 s to 0.8 s, the peak acceleration and maximum vertical displacement decrease by 51.1% and 22.7%, respectively. In contrast, the walking route has minimal effect on the dynamic response at the center of the slab.

Keywords

Vibration characteristics, long-span, reinforced concrete hollow flat slabs

INTRODUCTION

With the continuous advancement of urbanization in China, the application of long-span structures in practical engineering has become increasingly widespread. In recent years, a novel cast-in-situ reinforced concrete hollow flat slab system has been extensively adopted in practical engineering projects [1]. This slab system offers significant advantages, including rapid construction, reduced formwork usage, and efficient space utilization. Figure 1 illustrates the construction process of the slab: first, the bottom reinforcement is laid on the formwork; then, the built-in modules are placed; followed by the installation of tie bars and top reinforcement; finally, concrete is poured.

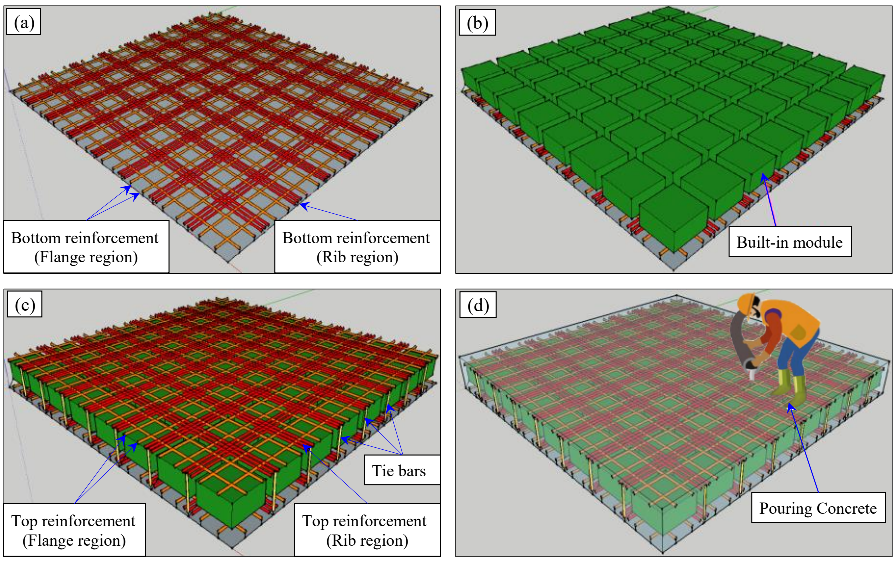

Figure 1 Construction process of slabs: (a) Tying bottom reinforcements, (b) Placing built-in modules, (c) Tying tie bars and top reinforcements, (d) Pouring concrete

Given the broad application prospects of the reinforced concrete hollow flat slab, numerous scholars have conducted extensive experimental and theoretical research on this floor structural system. Zhou et al. [1] conducted a detailed analysis of the internal forces in reinforced concrete hollow flat slabs under vertical loads. The study revealed that the internal forces in the slab are closely related to the stiffness of the supporting beams. Specifically, greater beam stiffness leads to a more uniform distribution of internal forces within the slab. Zhang et al. [2] conducted field experimental studies and numerical simulations on the mechanical behavior of reinforced concrete hollow flat slabs. Their investigation revealed a notable dual characteristic in stress distribution, described as "banded gradient" and "island-like concentration." Stresses were found to be particularly concentrated near the column edges, reflecting the load transfer path within the slab system. Zeng et al. [3] conducted experimental and numerical analyses on the flexural performance of a precast modular reinforced concrete hollow flat slab. Their study revealed that cracks were predominantly concentrated at the module joints. When the load reached 16.63 kN/m², an “X-shaped” crack pattern formed on the slab surface. At this stage, the reinforcement had not yet yielded, demonstrating that the slab possesses sufficient safety redundancy. In addition, other scholars have conducted extensive research on various aspects of similar flat slab structures, including material properties, construction methods, and structural performance [4-10].

Typically, floor systems are designed for static actions. However, dynamic actions are also critically important, as they account for numerous structural failures. To satisfy the serviceability limit state criteria, structures must maintain their functionality under in-service loads and should not cause discomfort to occupants during daily activities [11]. It is important to note that in long-span floor systems, their vibrational effects become significantly more pronounced. For this reason, the Chinese code GB 50010 [12] explicitly requires an analysis of floor vibration serviceability to ensure occupant comfort. To date, researchers have conducted extensive investigations into the vibration performance of long-span concrete slabs [13], steel floors [14], timber floors [15], and steel–concrete composite floors [16]. However, existing vibration studies have seldom addressed reinforced concrete hollow flat slabs, particularly in large-span applications. Therefore, it is imperative to undertake an in-depth examination of the vibration characteristics of this specific type of floor system.

In this study, the vibration characteristics of a long-span reinforced concrete hollow flat slab are thoroughly investigated based on the design practice of an actual engineering project. The effects of various factors, including slab thickness, supporting beam cross-sectional dimensions, and excitation loads, are taken into consideration. A detailed analysis is conducted on key dynamic properties, such as the natural frequency and peak acceleration of the flat slab system. The findings are expected to provide valuable references for the engineering design of this type of floor system.

BUILDING INFORMATION

The building under study is located in Dushan County, Guizhou Province, China. It serves as the office building of a commercial bank, with a total of 16 floors and an overall structural height of 66.5 meters, as shown in Figure 2(a). Within this building, the second floor is designed as a commercial service area, employing a long-span reinforced concrete hollow flat slab system. The post-construction actual views of these areas are illustrated in Figures 2(b) and (c), respectively.

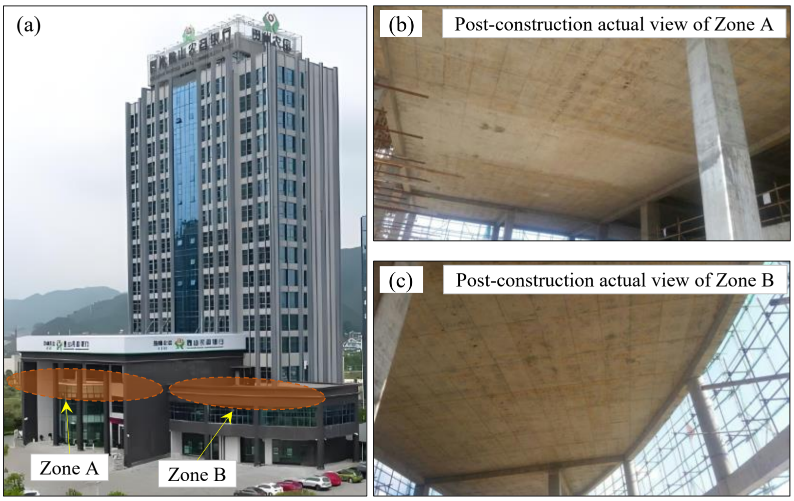

Figure 2 The studied building case: (a) Locations of long-span floor zones, (b) Actual view of Zone A, (c) Actual view of Zone B

The floor plan of the long-span hollow flat slab is shown in Figure 3(a). Zone A in the figure serves as the banking operation center, accommodating a high volume of personnel activities. Zone B serves as an accessible roof terrace, providing a rest area for bank customers. The shorter span of the long-span Zone A is 15.6 m, while the longer span is 23.4 m. The long-span Zone B has an irregular planar geometry, with the two directional spans being relatively close in dimension. The cross-sectional details of the slab in the long-span area and the non-long-span area are illustrated in Figures 3(b) and (c), respectively. Based on the availability of materials in the local market, C35-grade concrete is adopted for the long-span reinforced concrete hollow flat slab in this project, with an axial compressive strength of 23.4 MPa. HRB400-grade steel reinforcement is employed, exhibiting a yield strength of 400 MPa.

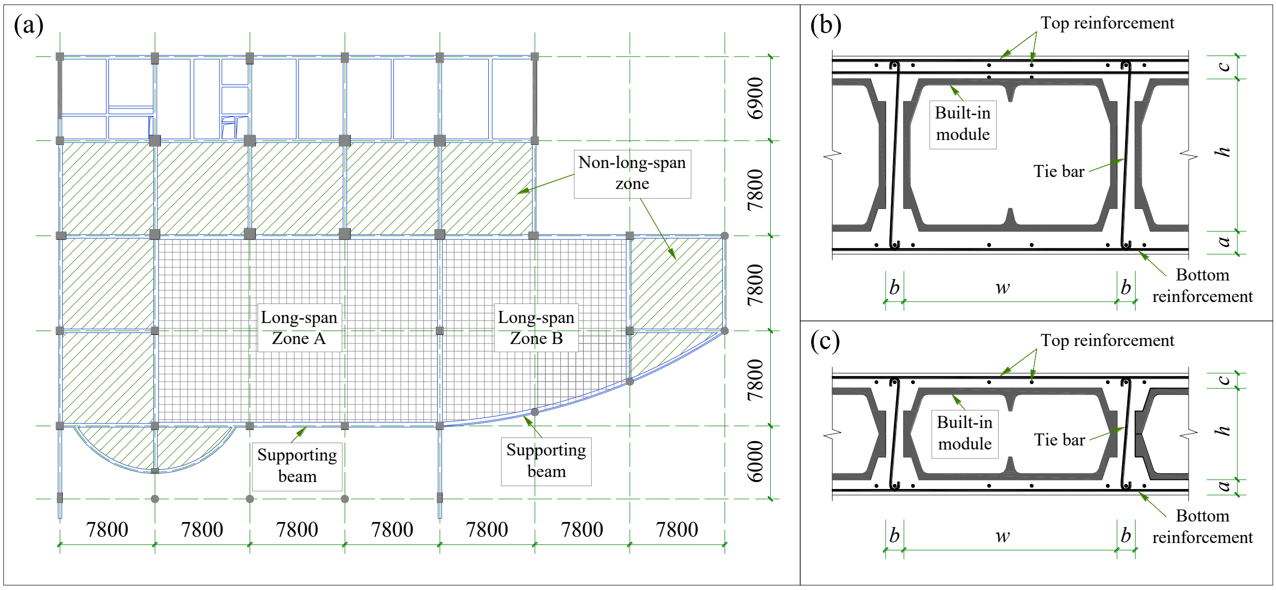

Figure 3 Design information of the building case: (a) Floor plan, (b) Cross-section of the long-span slab, (c) Cross-section of the non-long-span slab

DYNAMIC CHARACTERISTICS OF SLABS

Existing studies have indicated that factors such as floor span, stiffness, and support conditions significantly influence the dynamic characteristics of floor slabs [17-20]. Accordingly, this study investigates the dynamic properties of reinforced concrete hollow flat slabs by examining parameters such as the cross-sectional height of the slab and the cross-sectional dimensions of the supporting beams. A total of nine numerical models were established for the analysis, with the relevant design parameters provided in Table 1. Among them, Model M-03 was selected as the reference model. The supporting beams refer to those of the long-span hollow flat slab, which are arranged along the perimeter of the hollow flat slab. In this study, the finite element simulation software LBSSD, a specialized tool for floor vibration serviceability analysis, was employed for the simulation. Beams and columns were modeled using spatial beam elements, while the floor slab was modeled using shell elements. Fixed constraints were applied to the bottoms of all vertical members. Based on preliminary trial calculations, the mesh density of the floor system was set to 0.2 m.

Table 1 Design parameters of numerical models

Model No.	Slab section in long-span zone (mm)					Slab section in non-long-span zone (mm)					Supporting beam
	a	*b*	*c*	*w*	*h*	*a*	*b*	*c*	*w*	*h*	(mm×mm)
M-01	75	80	75	700	**300**	50	80	50	700	300	400×1000
M-02	75	80	75	700	**400**	50	80	50	700	300	400×1000
M-03	75	80	75	700	**500**	50	80	50	700	300	400×1000
M-04	75	80	75	700	**600**	50	80	50	700	300	400×1000
M-05	75	80	75	700	**700**	50	80	50	700	300	400×1000
M-06	75	80	75	700	500	50	80	50	700	**200**	400×1000
M-07	75	80	75	700	500	50	80	50	700	**400**	400×1000
M-08	75	80	75	700	500	50	80	50	700	300	**400×800**
M-09	75	80	75	700	500	50	80	50	700	300	**400×1200**

A harmonic excitation load was applied at the mid-span of the long-span zone A in all numerical models. The mode shapes of all orders exhibited minimal variation across different models, as illustrated in Figure 4. Among these, the first mode shape demonstrated a globally synchronized vertical bending deformation, characterized by a dome-shaped surface. The deformation was primarily concentrated in the long-span zone A, with the maximum displacement occurring at the center of the slab in this region. The second mode shape similarly exhibited a globally synchronized vertical bending deformation. The deformation was predominantly observed in the long-span zone B, with the maximum displacement located at the center of the slab in this region. The third mode shape was characterized by deformation primarily concentrated in the long-span zone A. Along the longitudinal direction of this slab span, the deformation partitioned the slab into two regions exhibiting anti-phase vertical motions.

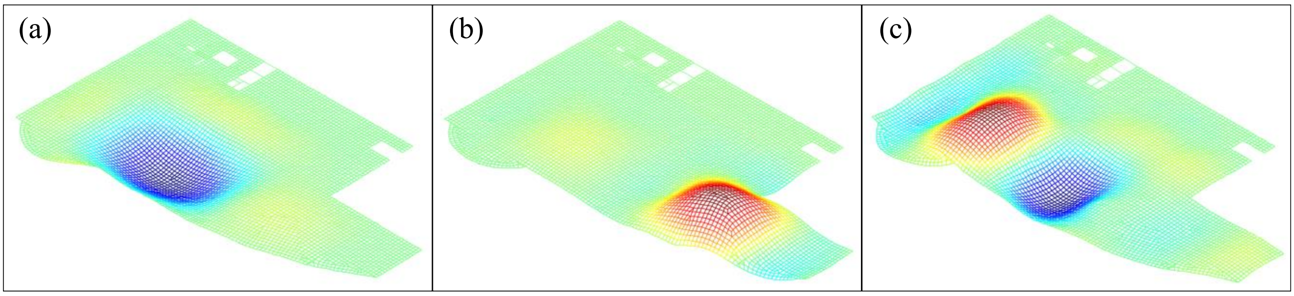

Figure 4 Mode shapes of reinforced concrete hollow flat slabs: (a) The first mode shape, (b) The second mode shape, (c) The third mode shape

The fundamental frequencies of all numerical models are presented in Figure 5. Figure 5(a) illustrates the influence of the slab cross-sectional dimensions in the long-span zone on the fundamental frequency of the floor system. As can be observed from the figure, the fundamental frequency of the floor increases with the height of the slab section. When the total sectional height is increased from 450 mm to 550 mm, 650 mm, 750 mm, and 850 mm, the fundamental frequency rises from 5.043 Hz to 5.814 Hz, 6.529 Hz, 7.206 Hz, and 7.847 Hz, representing increases of 15.3%, 29.5%, 42.9%, and 55.6%, respectively. Figure 5(b) illustrates the influence of the slab cross-sectional dimensions in the non-long-span regions on the fundamental frequency of the floor system. As shown in the figure, an increase in the slab sectional height within the non-long-span zones also leads to a corresponding improvement in the fundamental frequency, albeit to varying degrees. When the slab sectional height in these regions is increased from 300 mm to 400 mm and 500 mm, the fundamental frequency of the floor rises from 6.386 Hz to 6.529 Hz and 6.708 Hz, respectively. This behavior can be primarily attributed to the enhanced overall stiffness of the floor system resulting from the increased sectional height in the non-long-span zones, which consequently leads to an elevation in the fundamental frequency. Figure 5(c) illustrates the influence of the cross-sectional dimensions of the supporting beams on the fundamental frequency of the floor system. As can be observed from the figure, variations in the cross-sectional size of the supporting beams have a relatively minor effect on the fundamental frequency. When the beam cross-section is increased from 400 mm × 800 mm to 400 mm × 1000 mm and further to 400 mm × 1200 mm, the fundamental frequency of the floor experiences only marginal improvements of 0.7% and 1.3%, respectively.

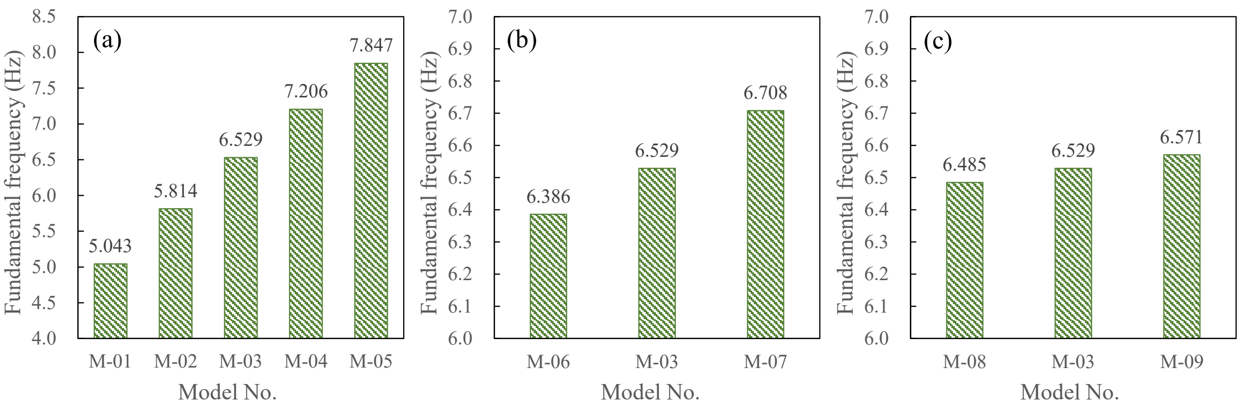

Figure 5 Fundamental frequencies of reinforced concrete hollow flat slabs: (a) Effect of slab section in long-span zone, (b) Effect of slab section in non-long-span zone, (c) Effect of supporting beam section

DYNAMIC RESPONSE OF SLABS UNDER HUMAN-INDUCED LOADS

Using the M-03 model as the analysis object, various human-induced loads were applied. The load model for a single walking step is shown in Figure 6(a). When applying a single-step load at the center of long-span zone A, both the magnitude of the applied load and the duration of the single step were considered as variables. Liu et al. [16]

investigated the one-step walking model based on 150 walking tests and found that the maximum walking load was approximately 0.9 kN. According to the relationship between human weight and walking load, the variable range of the weight excitation parameters in this study was taken as 0.4 kN to 0.8 kN. The statistical results also showed that the load duration did not exceed 0.87 s, with a mean value of 0.62 s. Therefore, the variable range of the load duration in this study was taken as 0.4 s to 0.8 s. For continuous walking loads applied in the long-span area, three walking routes were selected, as illustrated in Figure 6(b). Racic et al. [21] reviewed human walking speeds and found that the comfortable walking speed for adults is 1.5 m/s. Therefore, this value was adopted as the walking speed in the continuous walking analysis.

Figure 7 illustrates the dynamic response at the center of the floor slab under different gravity excitations. As shown in Figure 7(a), the variation patterns of the acceleration time-history curves for the floor under various gravity excitations are generally consistent. The greater the applied gravity excitation, the larger the peak acceleration of the floor. When the applied gravity increases from 0.4 kN to 0.6 kN and 0.8 kN, the peak acceleration increases from 1.426 mm/s² to 2.145 mm/s² and 2.864 mm/s², representing growth rates of 50.4% and 100.8%, respectively. This indicates that the peak acceleration is proportional to the magnitude of the applied gravity. Figure 7(b) shows the vertical displacement at the center of the slab. As can be observed from the figure, the variation patterns of the vertical displacement time-history curves under different gravity excitations are also fundamentally consistent. The greater the applied gravity excitation, the larger the maximum vertical displacement. When the applied gravity increases from 0.4 kN to 0.6 kN and 0.8 kN, the maximum vertical displacement increases from 2.578 × 10^{-3} mm to 3.869 × 10^{-3} mm and 5.161 × 10^{-3} mm, representing growth rates of 50.1% and 100.2%, respectively. This indicates that the maximum vertical displacement is also proportional to the magnitude of the applied gravity.

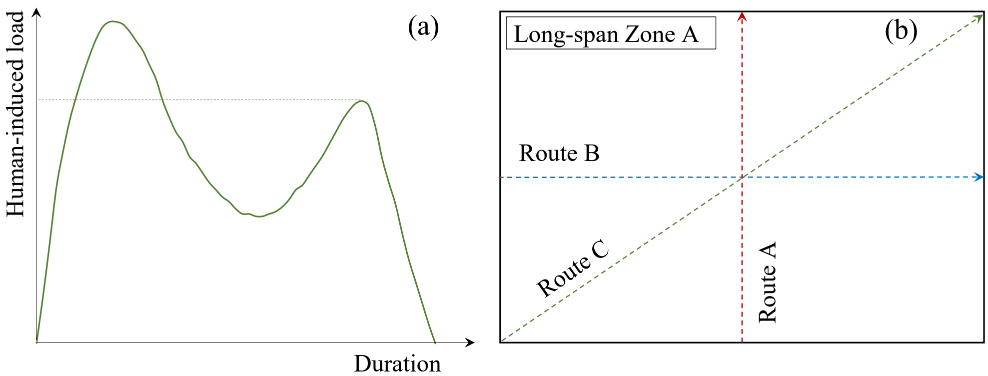

Figure 6 Human-induced loads: (a) Load model for a single walking step, (b) Walking routes

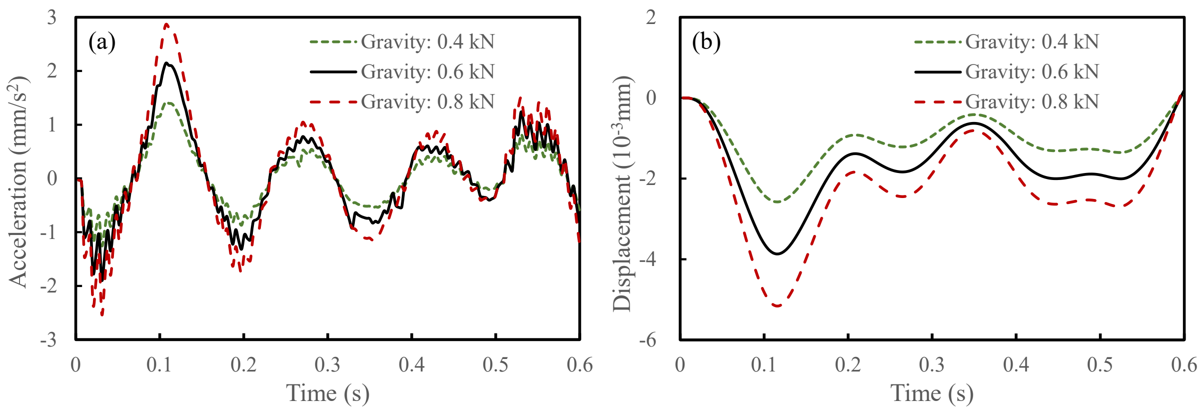

Figure 7 Dynamic response of floor slab under different gravity excitations: (a) Vertical acceleration, (b) Vertical displacement

Figure 8 illustrates the dynamic response of the floor slab under varying durations of a single-step load. As can be seen from Figure 8(a), the variation patterns of the vertical acceleration under different load durations are generally consistent. However, the shorter the duration of the single-step load, the greater the acceleration of the floor slab. When the load duration increases from 0.4 s to 0.6 s and 0.8 s, the peak acceleration decreases from 3.386 mm/s² to 2.145 mm/s² and 1.656 mm/s², representing reductions of 36.7% and 51.1%, respectively. Overall, the peak acceleration is inversely proportional to the load duration. Figure 8(b) presents the time-history curve of the vertical displacement at the center of the floor slab. It can be observed from the figure that the time at which the maximum vertical displacement occurs remains largely consistent across different load durations. The shorter the duration of the single-step load, the greater the maximum vertical displacement of the floor slab. When the load duration increases from 0.4 s to 0.6 s and 0.8 s, the maximum vertical displacement decreases from 4.374 × 10^{-3} mm to 3.869 × 10^{-3} mm and 3.379 × 10^{-3} mm, corresponding to reductions of 11.5% and 22.7%, respectively.

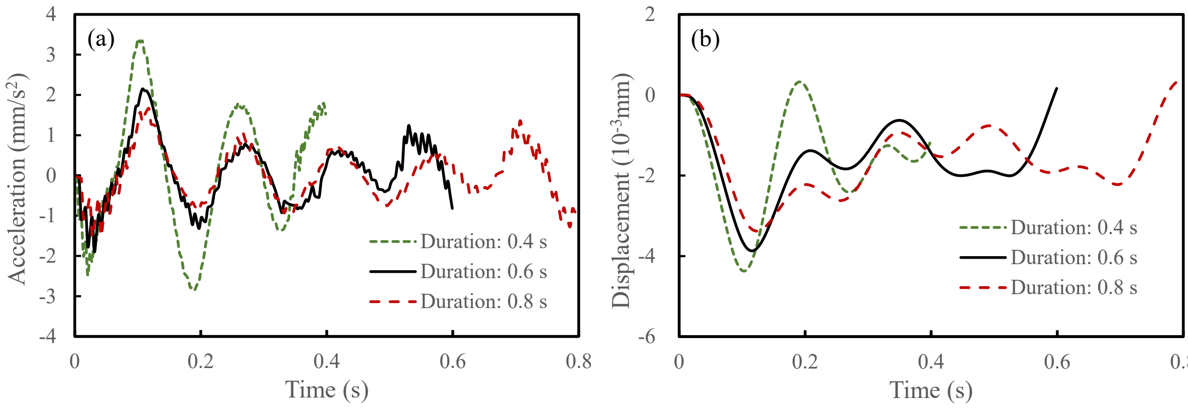

Figure 8 Dynamic response of floor slab under different load durations: (a) Vertical acceleration, (b) Vertical displacement

A walking excitation with a gravity load of 0.6 kN, a single-step duration of 0.6 s, and a walking speed of 1.5 m/s was applied within the long-span zone A. Route A follows the short-span direction of the long-span area, Route B follows the long-span direction, and Route C follows the diagonal direction. Figure 9 shows the envelope of the vertical accelerations of the floor. It can be observed that under the walking excitation along Route A, areas with larger accelerations are mainly distributed along the outer sides of the long-span region. This is because the periphery of the long-span area acts as the edge of the entire floor system, providing relatively limited constraint to the long-span slab. Under the walking condition along Route B, regions with higher accelerations primarily occur in the central part of the long-span floor. For excitation along Route C, areas of greater acceleration exhibit a diagonal distribution pattern and also exert varying degrees of influence on adjacent floor regions near the corners.

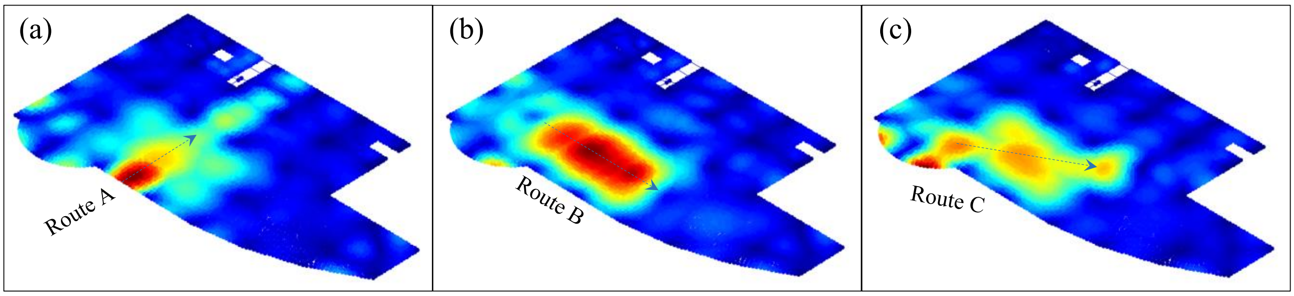

Figure 9 Vertical acceleration envelope of the floor: (a) Route A, (b) Route B, (c) Route C.

Figure 10 illustrates the dynamic response of the floor under different walking routes. Among them, Figure 10(a) shows the acceleration time-history curves at the center of the floor for the three walking modes. It can be observed that the overall shape of the time-history curves is spindle-like, with larger acceleration values in the central region of the graph. This occurs because half of the total walking duration corresponds to the moment when the walker reaches the center of the long-span area. Furthermore, the peak accelerations under the three walking modes show little variation. The peak accelerations corresponding to Route A, Route B, and Route C are 0.929 mm/s², 0.922 mm/s², and 0.912 mm/s², respectively, indicating that the walking path has no significant influence on the peak acceleration. Figure 10(b) presents the vertical displacement at the center of the floor under the three walking modes. Judging from the characteristics of the vertical displacement time-history curves, all three curves exhibit a tongue-shaped profile, where the vertical displacement is relatively small at the beginning and end of the walking process and reaches its peak when half of the total walking duration has elapsed. This phenomenon occurs because the walker reaches the center of the long-span area at that moment. Moreover, the maximum vertical displacement at the center of the floor shows little difference among the three walking modes. The maximum vertical displacements corresponding to Route A, Route B, and Route C are 3.238 × 10^{-3} mm, 3.268 × 10^{-3} mm, and 3.264 × 10^{-3} mm, respectively, indicating that the walking route has limited influence on the maximum vertical displacement of the floor.

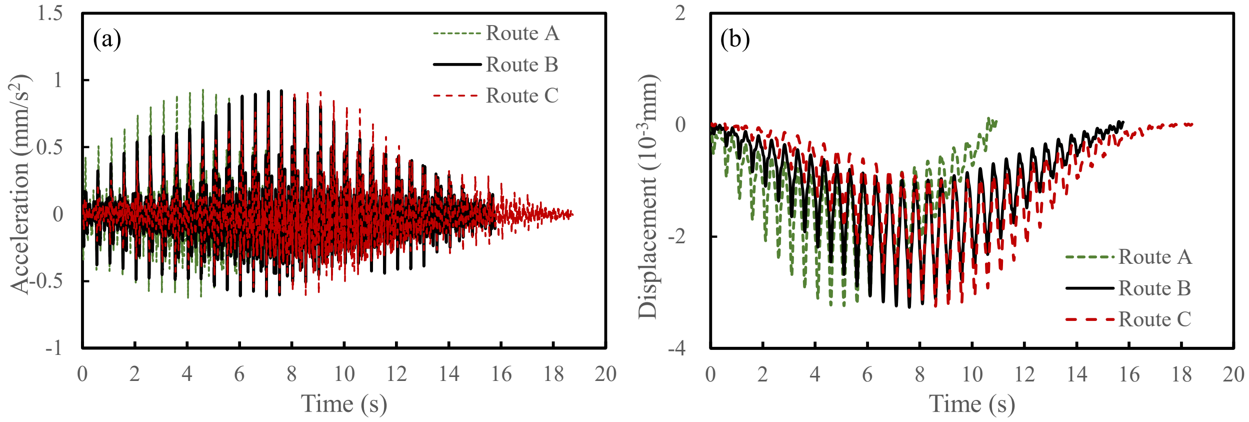

Figure 10 Dynamic response of floor slab under different walking routes: (a) Vertical acceleration, (b) Vertical displacement

The Chinese code GB 50010 [12] specifies clear requirements for floor vibration serviceability. For floors that serve as the banking operation center, the limit for peak acceleration is set at 0.05 m/s², and the natural frequency of the floor must be greater than or equal to 3 Hz. It can be concluded that the dynamic responses of the reinforced concrete hollow flat slab studied in this research fully comply with the relevant provisions of GB 50010 [12], see Table 2. This demonstrates that the reinforced concrete hollow flat slab exhibits favourable vibration serviceability performance, highlighting its potential for practical application and wider adoption in engineering projects.

Table 2 Comparison between the calculated dynamic response and the limit value specified in GB 50010

Item	Model No. / Human-induced vibration excitation	Calculated value	Value recommended by GB 50010
Fundamental frequency	M-01	5.043 Hz	≥ 3 Hz
	M-02	5.814 Hz	
	M-03	6.529 Hz	
	M-04	7.206 Hz	
	M-05	7.847 Hz	
	M-06	6.386 Hz	
	M-07	6.708 Hz	
	M-08	6.485 Hz	
	M-09	6.571 Hz	
Peak acceleration	M-03 / Applied gravity=0.4 kN	1.426 mm/s²	≤ 0.05 m/s² (50 mm/s²)
	M-03 / Applied gravity=0.6 kN	2.145 mm/s²	
	M-03 / Applied gravity=0.8 kN	2.864 mm/s²	
	M-03 / Load duration=0.4 s	3.386 mm/s²	
	M-03 / Load duration=0.6 s	2.145 mm/s²	
	M-03 / Load duration=0.8 s	1.656 mm/s²	
	M-03 / Walking mode=Route A	0.929 mm/s²	
	M-03 / Walking mode=Route B	0.922 mm/s²	
	M-03 / Walking mode=Route C	0.912 mm/s²	

CONCLUSIONS

In this study, a long-span hollow flat slab engineering case was investigated, analyzing the vibration characteristics of the floor and examining its dynamic response under human-induced vibration loading. The main research findings are summarized as follows.

1. The slab thickness in both the long-span zone and the non-long-span zone significantly influences the fundamental frequency of the floor. Specifically, a greater slab thickness results in a higher fundamental frequency. Fundamental frequency increased from 5.043 Hz to 7.847 Hz when the slab thickness in the long-span zone increased from 450 mm to 850 mm (55.6% increase). In contrast, the cross-sectional

dimensions of the supporting beams have a relatively minor effect on the fundamental frequency; increasing beam depth from 800 mm to 1200 mm changed the frequency by only 1.3%, which can be attributed to their short spans and consequently limited contribution to the overall support stiffness.
2. Under a single-step walking excitation load, an increase in the applied gravitational load leads to a corresponding increase in both the peak acceleration and the maximum vertical displacement of the floor. Peak acceleration doubled when the gravity load increased from 0.4 kN to 0.8 kN. Conversely, when the duration of the single-step walking load is extended, the peak acceleration of the floor decreases, and the maximum vertical displacement is also reduced to varying degrees.
3. A comparative analysis of the three walking models set in the long-span area indicates that different walking modes significantly influence the distribution of peak acceleration regions on the floor. The acceleration time-history curve at the center of the floor exhibits a spindle-shaped profile, while the vertical displacement time-history curve shows a tongue-shaped characteristic. However, under all three walking modes, the peak acceleration and vertical displacement values at the center of the floor demonstrate negligible differences. Thus, the walking route had a negligible influence on central slab response.

REFERENCES

[1] Zhou, L., Huang, Y., Chen, B., Luo, A. (2015). Static analysis of hollow floor with gypsum built-in module. Build. Sci., 31(9), 19–25. DOI: 10.13614/j.cnki.11-1962/tu.2015.09.004. (in Chinese)

[2] Zhang, Z., Chen, F., Yu, W., Sheng, J., Wei, L., Hu, A. (2025). Mechanical performance of square box-type core mold hollow floor slabs based on field tests and numerical simulation. Buildings, 15(16), 2948. DOI: 10.3390/buildings15162948.

[3] Zeng, X., Feng, Y., Ruan, S., Xu, M., Gong, L. (2023). Experimental and numerical study on flexural behavior of a full-scale assembled integral two-way multi-ribbed composite floor system. Buildings, 13(10), 2517. DOI: 10.3390/buildings13102517.

[4] Chebo, K. A., Temsah, Y., Abou Saleh, Z., Darwich, M., Hamdan, Z. (2022). Experimental investigation on the structural performance of single span hollow core slab under successive impact loading. Materials (Basel), 15(2), 599. DOI: 10.3390/ma15020599.

[5] Sahoo, S., Veerendar, C., Thammishetti, N., Suriya Prakash, S. (2023). Experimental and numerical study on behaviour of fibre reinforced lightweight hollow core slabs under different flexure to shear ratios. Structures, 50, 1264–1284. DOI: 10.1016/j.istruc.2023. 02.099.

[6] Sahoo, S., Veerendar, C., Suriya Prakash, S. (2023). Experimental and numerical studies on flexural behaviour of lightweight and sustainable precast fibre reinforced hollow core slabs. Constr. Build. Mater., 377, 131072. DOI: 10.1016/j.conbuildmat.2023. 131072.

[7] Jiang, Q., Wang, H., Feng, Y., Chong, X., Huang, J., Zhang, K., Yu, F. (2022). Out-of-plane flexural performance of concrete composite wide flat beam with hollow-core slabs. Structures, 41, 629–642. DOI: 10.1016/j.istruc.2022.05.054.

[8] Chen, X., Liu, Y., Ma, Q., Zhou, P., Liu, X., Lin, J. (2025). Finite element analysis of flexural performance of reinforced truss hollow composite concrete slabs. Sci. Rep., 15, 7057. DOI: 10.1038/s41598-025-91209-3.

[9] Han, C., He, H., Luo, Q., Zhao, Y., Zhang, J. (2024). Experimental and theoretical study on static performance of prefabricated steel-bar truss frame-precast concrete composite hollow-core slabs. Structures, 61, 105971. DOI: 10.1016/j.istruc.2024. 105971.

[10] Alali, A. A., Huang, Y., Tsavdaridis, K. D. (2024). Comparative life cycle assessment (LCA) of the composite prefabricated ultra-shallow slabs (PUSS) and hollow core slabs in the UK. J. Build. Eng., 96, 110588. DOI: 10.1016/j.jobe.2024.110588.

[11] Kozarić, L., Varju, Đ., Vojnić Purčar, M., Bursać, S., Čeh, A. (2022). Experimental investigations and numerical simulations of the vibrational performance of composite timber-lightweight concrete floor structures. Eng. Struct., 270, 114908. DOI: 10.1016/j.engstruct.2022.114908.

[12] The Ministry of Housing and Urban-Rural Development of the People's Republic of China. (2020). GB 50010-2020: Code for Design of Concrete Structures.

[13] Chen, J., Yan, S., Zhang, M. (2014). Vibration performance assessment of a long-span concrete floor using field measurements over a five-year period. Adv. Struct. Eng., 17(8), 1145–1158. DOI: 10.1260/1369-4332.17.8.1145.

[14] Armijos-Moya Dr, S. V., Larosche Principal, A., Sterns Principal, A. (2024). Floor vibrations of steel-framed floor systems due to rhythmic activities—case study. Struct. Eng. Int., 34(3), 414–425. DOI: 10.1080/10168664.2024.2305750.

[15] Piran, F., Karampour, H., Guan, H., Kumar, C., Li, H., Junior, G. C. (2025). Strengthening lightweight long-span timber floors: A study on vibration performance and human perception. Eng. Struct., 343, 121062. DOI: 10.1016/j.engstruct.2025.121062.

[16] Liu, J., Huang, S., Li, J., Frank Chen, Y. (2022). Vibration serviceability of large-span steel–concrete composite beam with precast hollow core slabs under walking impact. Engineering, 19, 93–104. DOI: 10.1016/j.eng.2021.04.025.

[17] Tewari, D., Senthil, K., Sharma, A. (2023). Evaluation of force and dynamic factor on reinforced concrete deck slab through the static and transient dynamic tests. Asian J. Civ. Eng., 24, 2229–2246. DOI: 10.1007/s42107-023-00637-x.

[18] Lago, F. S., Kripka, M., Salem, O., Pravia, Z. M. C. (2019). Experimental and analytical study of vibration parameters in waffle concrete slabs. Eng. Struct., 199, 109593. DOI: 10.1016/j.engstruct.2019.109593.

[19] Wang, L., Gong, G., Xia, J. (2024). Comparison of evaluations of human-induced floor vibration based on different design guidelines. Structures, 68, 107114. DOI: 10.1016/j.istruc.2024.107114.

[20] Chocholaty, B., Eser, M., Hoppe, K.-A., Wang, D., Marburg, S. (2023). Vibration response of a hybrid steel–timber building element with uncertain material and joint parameters. Arch. Civ. Mech. Eng., 24, 22. DOI: 10.1007/s43452-023-00819-z.

[21] Racic, V., Pavic, A., Brownjohn, J.M.W. (2009). Experimental identification and analytical modelling of human walking forces: Literature review. J. Sound Vib., 326, 1-49. DOI: 10.1016/j.jsv.2009.04.020.